Transport Analyses based on High-Energy Invariant Manifold Tubes and Low-Energy Singular Collision Orbits in the Planar Circular Restricted Three-Body Problem

Kenta Oshima (National Astronomical Observatory of Japan)

Abstract

The first part of the present paper reveals interplays among invariant manifolds emanating from planar Lyapunov orbits around the collinear Lagrange points L_1, L_2, and L_3 for high energies. Once the energetically forbidden region vanishes, the invariant manifolds together form closed separatrices bounding transit orbits in the phase space, deviating from the low-energy picture of invariant manifold tubes. Though the qualitatively different behavior of invariant manifolds emerges for high energies, associated transit orbits possess a common feature generalized from that of low-energy transit orbits. The second part extends our previous proposal of using singular collision orbits associated with the secondary to find trajectories reaching the vicinity of the secondary to low energies. Statistical analyses indicate that singular collision orbits are useful to find such transfer trajectories except for the very-low-energy regime. These results are numerically obtained in the Earth-Moon and Sun-Jupiter planar circular restricted three-body problems.

平面円制限三体問題における高エネルギー不変多様体チューブと低エネルギー衝突軌道に基づく遷移軌道解析

大島 健太 (国立天文台)

摘要

本論文は，平面円制限三体問題において非線形性が強い高エネルギー条件では，ラグランジュ点L_1，L_2，L_3に付随する不変多様体が互いに協働することで，相空間内に閉じたセパラトリクス構造を形成することを見出した．線形ダイナミクスに近い低エネルギー条件において，各ラグランジュ点に付随する不変多様体がチューブ構造を形成する従来の描像とは定性的に異なる結果であるが，低エネルギーから高エネルギー領域にまたがる統一的な理解を可能とする，ラグランジュ点に付随する遷移軌道の性質を一般化した基準を提案する．さらに，第二天体の中心に衝突する特異的な軌道の相空間構造に基づいて第二天体近傍を通過する軌道を同定する手法を，以前提案した高エネルギー領域から低エネルギー領域にまで拡張する．幅広いエネルギー領域において提案手法は有効であるが，超低エネルギー領域においてのみ衝突軌道の大部分は第二天体近傍を脱出できないため計算効率が悪いので，ラグランジュ点に付随する不変多様体の相空間構造に基づく従来手法が有利であることがわかった．

1. Introduction

Stable and unstable manifolds emanating from planar Lyapunov orbits around the collinear Lagrange points have been a fundamental basis for understanding transport phenomena of asteroids, comets, and spacecrafts in the planar circular restricted three-body problem (CR3BP). Conley (1968)[1] investigated linearized dynamics near the collinear Lagrange points L_1 and L_2, and showed that transit orbits passing through equilibrium regions must be inside invariant manifold tubes in the phase space. Moser's theorem[2] assures that all the results obtained in such linear analyses qualitatively hold true in certain nonlinear regimes. Recently, Swenson et al. (2018)[3] quantitatively found that invariant manifold tubes govern transit orbits for energies at least as high as those of triangular Lagrange points (the Jacobi constant C=3) in the planar CR3BP. Two-dimensional invariant manifold tubes, which play the role of separatrices between transit and non-transit orbits in the three-dimensional energy surface, have been useful to find trajectories reaching the vicinity of the secondary in the low-energy regime. Transit orbits have been found from the phase-space region enclosed by a closed curve of invariant manifolds on a suitable Poincaré section. On the other hand, our previous study[4] found that, for higher energies of $C \leq 3$, invariant manifolds emanating from planar Lyapunov orbits around L_1 and L_2 do not form closed curves on a Poincaré section, which resulted in difficulties of identifying transfer trajectories reaching the vicinity of the secondary. This was the reason we proposed the use of singular collision orbits passing through the center of the secondary, based on the Levi-Civita regularization[5], to find desired transfer trajectories from the vicinity of phase-space structures of the singular collision orbits on a Poincaré section.

The present paper explores deeper into the implications in Oshima et al. (2017)[4] . The first part reveals interplays among invariant manifolds emanating from planar Lyapunov orbits around the three collinear Lagrange points L_1, L_2, and L_3 for high energies of $C \leq 3$. Once the energetically forbidden region vanishes, they together

form closed separatrices on a Poincaré section, diverging from the low-energy picture that an invariant manifold tube associated with a planar Lyapunov orbit around a single equilibrium point bounds transit orbits. High-energy transit orbits enclosed by the separatrices possess a common feature generalized from that of low-energy transit orbits. The generalization of criteria for transit orbits is also a contribution of this work.

Although transit orbits are enclosed by invariant manifolds in the phase space, they do not necessarily reach the vicinity of the secondary. The distance from the secondary depends on the energy level (size of Lyapunov orbits) and even low-energy transit orbits of C>3 can experience distant pathways from the secondary. However, trajectories reaching the vicinity of the secondary are often of great importance to astrodynamics and celestial mechanics. The second part of the present paper extends our previous proposal in Oshima et al. (2017)[4], of using singular collision orbits associated with the secondary to find trajectories reaching the vicinity of the secondary, to low energies. This study statistically investigates reachabilities and time of flights of singular collision orbits from the secondary to a Poincaré section, and shows that singular collision orbits are useful to find trajectories reaching the vicinity of the secondary, except for the very-low-energy regime.

The remainder of the paper is organized as follows. Section 2 summarizes the backgrounds. Section 3 unveils interplays among invariant manifolds emanating from planar Lyapunov orbits around L_1, L_2, and L_3 for high energies of C≤3. Section 4 presents statistical analyses on reachabilities and transfer times of singular collision orbits. Section 5 provides concluding remarks.

2. Backgrounds

2.1 Planar circular restricted three-body problem

The planar, circular, restricted, three-body problem (CR3BP) describes the motion of a massless particle P_3 under the gravitational influences of two bodies P_1 (primary) and P_2 (secondary) of masses m_1 and m_2 ($m_1 > m_2$), respectively. This model assumes that P_1 and P_2 revolve in circular orbits around their barycenter and P_3 moves on the orbital plane of P_1 and P_2. The equations of motion for P_3 in the P_1- P_2 rotating frame are (see Szebehely (1967)[6] for details)

$\ddot{x} - 2\dot{y} = -\partial\bar{U}/\partial x, \ddot{y} + 2\dot{x} = -\partial\bar{U}/\partial y,$

where the effective potential

$\bar{U} = -\frac{1}{2}(x^2 + y^2) - \frac{1-\mu}{\sqrt{(x+\mu)^2+y^2}} - \frac{\mu}{\sqrt{(x-1+\mu)^2+y^2}} - \frac{1}{2}\mu(1-\mu),$

the lower alphabetic subscripts denote the partial differentiations with respect to the subscripts, $\mu = m_2/(m_1 + m_2)$ is the mass parameter, and P_1 and P_2 are located on the x-axis at x=-μ and x=1-μ, respectively. The equations of motion admit five equilibria called the Lagrange points and an integral of motion called the Jacobi constant:

$C = -(\dot{x}^2 + \dot{y}^2) - 2\bar{U}.$

The region in the configuration space satisfying $C + 2\bar{U} > 0$ defines the energetically forbidden region, which only exists for energies of C>3.

2.2 Computation of invariant manifolds

The following is a brief summary of the procedure for computing stable and unstable manifolds emanating from an unstable periodic orbit (see Koon et al. (2011)[7] for details).

On arbitrary state $\boldsymbol{x}(t)$ along a periodic orbit, states of stable manifolds and unstable manifolds can be approximated as

$\boldsymbol{x}^{s\pm}(\boldsymbol{x}(t)) = \boldsymbol{x}(t) \pm \varepsilon \boldsymbol{Y}^s(\boldsymbol{x}(t)),$

$\boldsymbol{x}^{u\pm}(\boldsymbol{x}(t)) = \boldsymbol{x}(t) \pm \varepsilon \boldsymbol{Y}^u(\boldsymbol{x}(t)),$

where $0 < |\varepsilon| \ll 1$ is a small perturbation and $\boldsymbol{Y}^s(\boldsymbol{x}(t))$ and $\boldsymbol{Y}^u(\boldsymbol{x}(t))$ are stable and unstable eigenvectors of the monodromy matrix associated with $\boldsymbol{x}(t)$, respectively.

One can then globalize stable and unstable manifolds by propagating $\boldsymbol{x}^{s\pm}(\boldsymbol{x}(t))$ and $\boldsymbol{x}^{u\pm}(\boldsymbol{x}(t))$ backward and forward in time, respectively. This study only computes stable manifolds and always regularizes about P_2 during the propagations to ensure numerical accuracy against close flybys. Hereafter, stable manifolds emanating from planar Lyapunov orbits around L_1, L_2, and L_3 are denoted as W_1^S, W_2^S, and W_3^S, respectively.

3. Linking low- to high-energy dynamics of invariant manifolds and transit orbits

3.1 Poincaré section

A Poincaré section is a fundamental tool to understand phase-space structures in this study. Though the setting of a Poincaré section would not be very essential from the dynamical viewpoint, some cares should be taken, due to the following three issues, to avoid visualizations unnecessary difficult to analyze:

- The section should be able to simultaneously visualize W_1^S, W_2^S, and W_3^S and singular collision orbits due to the interest of this study
- Smaller values of μ can make phase-space structures of W_1^S and W_2^S more twisted and stretched on a Poincaré section far from the secondary[3]
- Higher-energy trajectories typically possess more looping behaviors in the rotating frame, which can produce the possibility of both signs of a velocity component at the section as shown in Fig.1

The first issue indicates that a candidate section should be located at the certain fixed x-component, the suitable value of which is determined based on the second issue, through trial and error, that x=0 in the

Earth-Moon system and x=0.5 in the Sun-Jupiter system. A Poincaré section with a fixed value of x usually visualizes phase-space structures on the y-v_y plane with the prescribed sign of v_x in many of the previous studies. Low-energy trajectories typically do not exhibit looping behaviors, but the third issue indicates that ambiguities of signs of v_x on the section can arise for higher-energy trajectories investigated in this study. Fig.1 highlights that a loop of a high-energy trajectory causes intersections of different signs of v_x on the Poincaré section at x=0. Therefore, it is not meaningful to visualize all of the crossing points on the same y-v_y plane due to the ambiguities of signs of v_x.

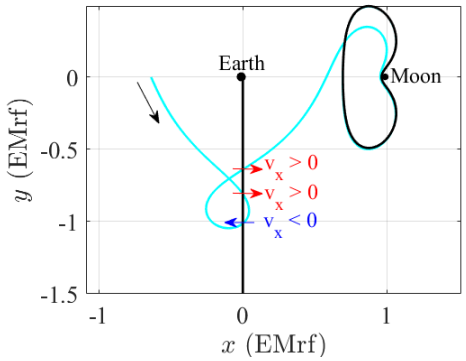

Fig. 1. An example of a high-energy trajectory (cyan) with C=2.95 having intersections with a Poincaré section at x=0 with different signs of v_x due to the loop in the Earth-Moon rotating frame (EMrf).

It is possible to classify phase-space structures based on signs of v_x, but employing $\theta_v = \tan^{-1}(v_y/v_x) \in [-\pi, \pi]$ instead of v_y enables visualizations in a single figure without ambiguities of signs[3] because the remaining variable is the magnitude of velocity, which is always not less than zero. To sum up, I set a Poincaré section at x=0 in the Earth-Moon system and x=0.5 in the Sun-Jupiter system, and visualize phase-space structures on the y-θ_v plane throughout this paper. Fig.2 shows the Poincaré section at x=0 and the energetically forbidden region in the Earth-Moon rotating frame (EMrf) with examples of (a) W_1^S, W_2^S, and W_3^S and (b) singular collision orbits emanating from the center of the Moon in the case of C=3.01. Hereafter, EMrf and SJrf abbreviate Earth-Moon and Sun-Jupiter rotating frames, respectively. I allow multiple intersections with the Poincaré section for a single trajectory with looping behaviors as illustrated in Fig.1 when visualizing phase-space structures. To simplify the analyses, I stop propagation if a trajectory is sufficiently far from the section: at x=0 with y<0 for W_1^S and W_2^S in the both systems, at x=0.7 for W_3^S in the Earth-Moon system, and at x=0.9 for W_3^S in the Sun-Jupiter system. Therefore, long-distance stable manifolds having intersections with the Poincaré section with both signs of y are out of the scope of the present paper. The later sections present phase-space structures on the Poincaré section in detail.

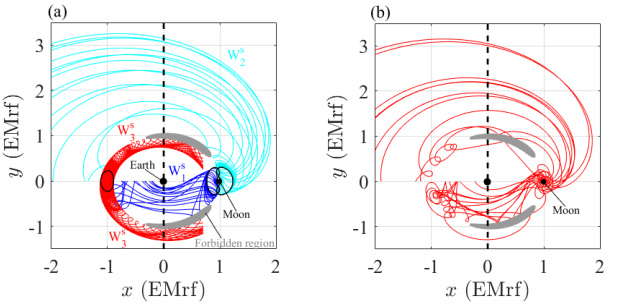

Fig. 2. The Poincaré section (the broken line) at x=0 and the energetically forbidden region (gray) in the Earth-Moon rotating frame (EMrf) with examples of (a) W_1^S (blue), W_2^S (cyan), and W_3^S (red) and (b) singular collision orbits emanating from the center of the Moon in the case of C=3.01.

3.2 Generalized criteria for transit orbits

This section proposes generalized criteria for identifying transit orbits associated with W_1^S, W_2^S, and W_3^S to aid analyses of transit orbits in high-energy regimes, where the definition of the equilibrium region based on the existence of the energetically forbidden region[1), 7)] is unclear. The generalization of criteria is based on well-understood low-energy transit orbits with the purpose of applying them to identify transit orbits in high-energy regimes.

Fig.3 (a) shows two typical types (I and II) of low-energy transit orbits inside a stable manifold tube of W_1^S with C=3.1. Since the type-I transit orbit is outside a stable manifold tube of an L_2 planar Lyapunov orbit, it crosses y=0 with x>1-μ and returns to the interior realm. The condition y=0 with x>1- μ is useful for identifying type-I transit orbits because they must pass through y=0 with x>1- μ to go back to the interior realm. On the other hand, the type-II transit orbit is inside the stable manifold tube of an L_2 planar Lyapunov orbit and reaches the exterior realm through the vicinity of the secondary (Moon in this case).

Fig.3(b) shows the associated time evolutions of the Kepler energy around the primary (Earth in this case). The relationship with the semi-major axis indicates that K=-0.5 approximately divides the interior (K<-0.5) and exterior (K>-0.5) realms. However, this criterion is not reliable near the secondary due to the two-body nature of K and even some non-transit orbits can have spikes crossing K=-0.5 at flybys. Therefore, an appropriate signal of type-II transit orbits is such that K<-0.5 at initial time and K exceeds -0.5 at a point far from the secondary. Of course, perturbations of the secondary cause net changes in K.

Above discussions are applicable to initial conditions in the exterior realm inside a stable manifold tube of W_2^S

in a similar manner. In summary, I propose the following two criteria (I and II) to identify transit orbits:

I. A trajectory of the initial condition K<-0.5 (or K>-0.5) crosses y=0 with $1-\mu < x < x_{L2}$ (or $x_{L1} < x < 1-\mu$)

II. A trajectory of the initial condition K<-0.5 (or K>-0.5) has K>-0.5 (or K<-0.5) at $r2>x_{L2} - x_{L1}$

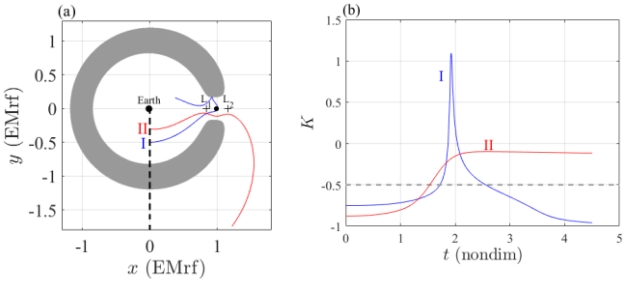

Fig. 3. (a) Two typical types (I and II) of low-energy transit orbits inside a manifold tube of W_1^S with C=3.1 and (b) the associated time evolutions of the Kepler energy around the Earth.

3.3 Phase-space structures

I perform grid searches to verify the validity of the proposed criteria for transit orbits. Throughout this paper, initial conditions are distributed on the y-θ_v plane on 1,000X1,000 rectilinear grids at the Poincaré section x=0 in the Earth-Moon system and at x=0.5 in the Sun-Jupiter system. I regularize the equations of motion about the secondary during propagation and stop propagation if one of the following conditions is satisfied: propagation time exceeds 365 days in the Earth-Moon system and 188.4 years in the Sun-Jupiter system; a trajectory collides with the surface of the primary; a trajectory of the initial condition y>0 returns to the section with y<0; a trajectory of the initial condition y<0 returns to the section with y>0.

3.3.1 Earth-Moon system

Fig.4 shows phase-space structures of W_1^S (blue), W_2^S (cyan), and W_3^S (red) with (a) C=3.1 and (b) C=3.01 at the Poincaré section x=0 in the Earth-Moon system. The figure also includes initial conditions of transit orbits (yellow), which satisfy at least one of the criteria, found via the grid search. Fig.4 (a) validates the criteria in the sense that W_1^S and W_2^S enclose all of the transit orbits satisfying at least one of the criteria without exceptions. At the energy level (b) C=3.01 higher than L_3, the energetically forbidden region separates W_1^S and W_3^S at y<0, and W_2^S and W_3^S at y>0. W_1^S, W_2^S, and W_3^S independently enclose the transit orbits with the aid of the energetically forbidden region.

It is interesting to note that the transit orbits enclosed by W_3^S also satisfy one of the criteria, whereas the criteria are originally defined based on transit orbits associated with W_1^S and W_2^S. Fig.5 (a) shows typical transit orbits propagated forward in time from initial conditions inside a stable manifold tube of W_3^S with C=3.01 in Fig.4(b). The trajectories exhibit tadpole motions because W_3^S separates tadpole-type captured orbits from non-captured orbits[8]. Since tadpole orbits switch between K>-0.5 and K<-0.5 driven by perturbations of the secondary[9], as also shown in Fig.5 (b), transit orbits enclosed by W_3^S actually satisfy the criterion II.

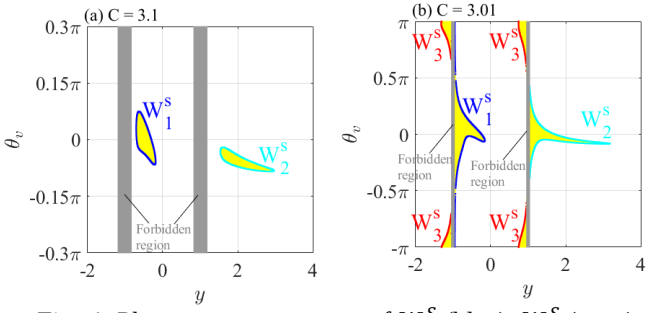

Fig. 4. Phase-space structures of W_1^S (blue), W_2^S (cyan), and W_3^S (red) with (a) C=3.1 and (b) C=3.01 at the Poincaré section x=0 in the Earth-Moon system. The figure also includes initial conditions of transit orbits (yellow), which satisfy at least one of the criteria.

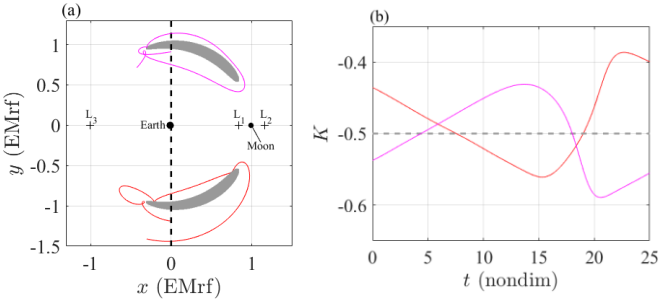

Fig. 5. (a) Two typical transit orbits inside a manifold tube of W_3^S with C=3.01 and (b) the associated time evolutions of the Kepler energy around the Earth.

Fig.6 shows phase-space structures of W_1^S (blue), W_2^S (cyan), and W_3^S (red) with (a) C=3 and (b) C=2.95 at the Poincaré section x=0 in the Earth-Moon system. Once the energetically forbidden region vanishes, W_1^S, W_2^S, and W_3^S no longer independently enclose transit orbits. Instead, they together form closed separatrices bounding transit orbits, which satisfy at least one of the criteria. This situation is qualitatively the same for the higher energy level (d) C=2.95. The strong nonlinearity for high energies causes the divergence from the linear prediction[1] that an invariant manifold tube associated with a Lyapunov orbit around a single equilibrium point bounds transit orbits, but now the interplays among W_1^S, W_2^S, and W_3^S bound transit orbits. Though the qualitatively different behavior of invariant manifolds emerges for high energies, it is still possible to

understand the common feature of transit orbits from low- to high-energy regimes in a unified manner based on the proposed criteria.

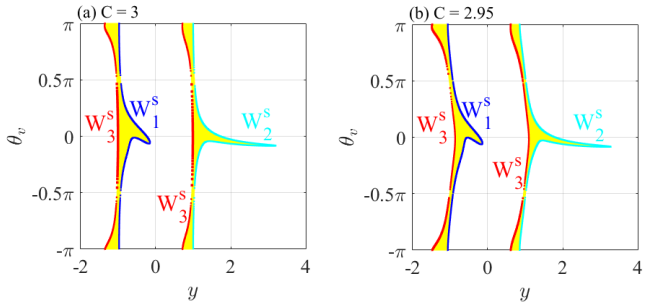

Fig. 6. Phase-space structures of W_1^S (blue), W_2^S (cyan), and W_3^S (red) with (a) C=3 and (b) C=2.95 at the Poincaré section x=0 in the Earth-Moon system. The figure also includes initial conditions of transit orbits (yellow), which satisfy at least one of the criteria.

3.3.2 Sun-Jupiter system

A question may arise whether the results presented in the previous section are peculiar to the Earth-Moon system or not. I apply the same procedure to the Sun-Jupiter system to confirm the universality of the interplays among W_1^S, W_2^S, and W_3^S and the validity of the proposed criteria for transit orbits.

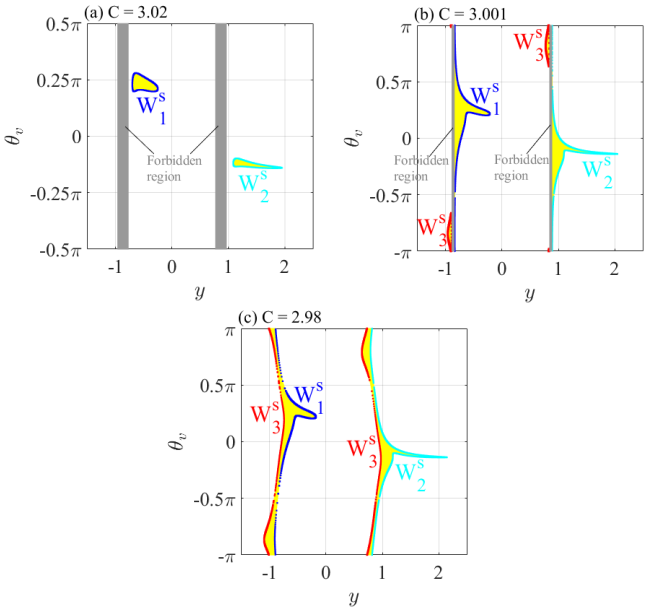

Fig. 7. Phase-space structures of W_1^S (blue), W_2^S (cyan), and W_3^S (red) with (a) C=3.02, (b) C=3.001, and (c) C=2.98 at the Poincaré section x=0.5 in the Sun-Jupiter system. The figure also includes initial conditions of transit orbits (yellow), which satisfy at least one of the criteria.

Fig.7 shows phase-space structures of W_1^S (blue), W_2^S (cyan), and W_3^S (red) with (a) C=3.02, (b) C=3.001, and (c) C=2.98 at the Poincaré section x=0.5 in the Sun-Jupiter system. The results are qualitatively same as those in the Earth-Moon system in the sense that W_1^S, W_2^S, and W_3^S independently enclose transit orbits for low energies of C>3, whereas they together form closed separatrices bounding transit orbits for high energies of C≤3. The results indicate that the transit orbits satisfy the criteria independent of energies also in the Sun-Jupiter system.

4. Linking high- to low-energy dynamics of singular collision orbits

The previous section has explored the dynamics of stable manifolds and associated transit orbits from low- to high-energy regimes. Although W_1^S, W_2^S, and W_3^S bound transit orbits, they do not necessarily reach the vicinity of the secondary according to the criteria. In practice, trajectories reaching the vicinity of the secondary, e. g., capture into low-altitude science orbits, swing-bys, and impacts of hazardous objects, are often of great importance in astrodynamics and celestial mechanics. Therefore, this section extends our previous proposal in Oshima et al. (2017)[4], of using singular collision orbits associated with the secondary to find trajectories reaching the vicinity of the secondary, to low energies.

Singular collision orbits are particularly useful for high energies to straightforwardly find trajectories reaching the vicinity of the secondary among various possible pathways including distant ones from the secondary. However, a question may arise whether singular collision orbits are useful for any energies or there is a limitation. The linear stability analysis of the origin in the Levi-Civita regularized coordinates[4] indicates difficulties for low-energy singular collision orbits to escape from the vicinity of the secondary, but it is still unclear how difficult for a certain value of the energy.

To explore this issue, the present study investigates reachabilities and time of flights (TOFs) of singular collision orbits from the center of the secondary to a Poincaré section at x=0 in the Earth-Moon system and x=0.5 in the Sun-Jupiter system for various values of the Jacobi constant. I propagate 1,000 singular collision orbits backward in time allowing multiple intersections for each collision orbit and stop propagation if one of the following conditions is satisfied: propagation time exceeds 365 days in the Earth-Moon system and 188.4 years in the Sun-Jupiter system; a trajectory reaches y=0 with x<0.

Reachabilities to the Poincaré section, for each case of y>0 and y<0, are simply assessed by a ratio of the number of unreachable collision orbits to the population. A cumulative distribution function (CDF) may be useful

for statistical analyses of TOFs from the secondary to the Poincaré section. I compute the empirical CDF in terms of TOFs for all of the intersections with the Poincaré section. As a benchmark value, I extract the TOF at which the CDF exceeds 0.5 for the first time (TOF_{half}).

Figs.8 and 9 present (a) the percentage of unreachable collision orbits and (b) the values of TOF_{half} in terms of Jacobi constants from high to low energies for the Poincaré sections with y>0 (red circle) and y<0 (blue star) in the Earth-Moon and Sun-Jupiter systems, respectively. The panels (a) show that singular collision orbits cannot reach the Poincaré sections for very-low-energy regimes and the panels (b) show that the values of TOF_{half} quickly increase once the energy becomes low enough. Note that high percentages of unreachable collision orbits and long TOFs require inefficient time-consuming computations. Nevertheless, the statistical properties indicate that singular collision orbits can be useful computational tools to find trajectories reaching the vicinity of the secondary from high to low energies except for the very-low-energy regime, where invariant manifolds emanating from Lyapunov orbits are more useful.

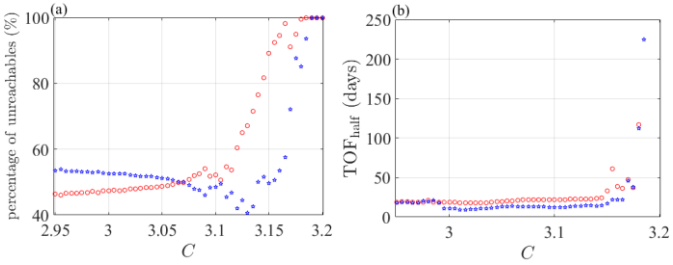

Fig. 8. (a) The percentage of unreachable collision orbits and (b) the values of TOF_{half} in terms of Jacobi constants for the Poincaré section x=0 with y>0 (red circle) and y<0 (blue star) in the Earth-Moon system. There are no plots in (b) for the energies that all of the collision orbits cannot reach the Poincaré section.

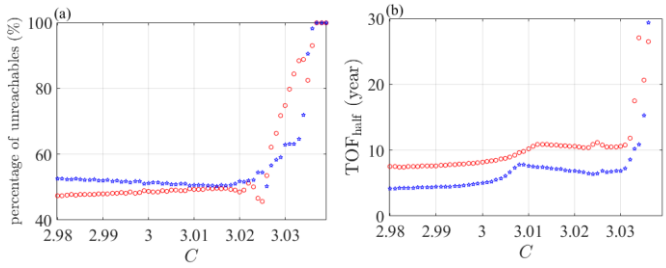

Fig. 9. (a) The percentage of unreachable collision orbits and (b) the values of TOF_{half} in terms of Jacobi constants for the Poincaré section x=0.5 with y>0 (red circle) and y<0 (blue star) in the Sun-Jupiter system. There are no plots in (b) for the energies that all of the collision orbits cannot reach the Poincaré section.

5. Conclusions

The numerical analyses on phase-space structures in the Earth-Moon and Sun-Jupiter planar CR3BPs have indicated that stable manifolds emanating from planar Lyapunov orbits around the three collinear points together form closed separatrices once the energetically forbidden region vanishes in the high-energy regime. High-energy transit orbits bounded by the stable manifolds satisfy the same criteria that low-energy transit orbits also satisfy. The statistical analyses in terms of reachabilities and time of flights have indicated that low-energy singular collision orbits can be similarly useful as high-energy ones to find trajectories reaching the vicinity of the secondary, except for the very-low-energy regime.

References

1) Conley, C. C.: Low energy transit orbits in the restricted three-body problems. SIAM Journal on Applied Mathematics 16, 732-746 (1968).
2) Moser, J.: On the generalization of a theorem of A. Liapounoff. Communications on Pure and Applied Mathematics 11, 257-271 (1958).
3) Swenson, T., Lo, M., Anderson, B., Gorordo, T.: The Topology of Transport Through Planar Lyapunov Orbits. Space Flight Mechanics Meeting, AIAA 2018-1692, Kissimmee, USA, 8-12 January (2018).
4) Oshima, K., Topputo, F., Campagnola, S., Yanao, T.: Analysis of medium-energy transfers to the Moon. Celest. Mech. Dyn. Astr. 127, 285-300 (2017).
5) Levi-Civita, T.: Sur la résolution qualitative du probleme restrient des trios corps. Acta Mathematica 30, 305-327 (1906).
6) Szebehely V., 1967, Theory of Orbits: The Restricted Problem of Three Bodies. Academic Press Inc, New York, USA
7) Koon W. S., Lo M.W., Marsden J. E., Ross S. D., 2011, Dynamical Systems, the Three-Body Problem and Space Mission Design. Marsden Books, Wellington, New Zealand
8) Oshima, K., Yanao, T.: Jumping mechanisms of Trojan asteroids in the restricted three- and four-body problems. Celest. Mech. Dyn. Astr. 122, 53-74 (2015).
9) Murray C. D., Dermott S. F., 1999, Solar System Dynamics. Cambridge University Press, New York, USA